Journal of Nuclear Materials 495 (2017) 442–454

Contents lists available at ScienceDirect

Journal of Nuclear Materials

journal homepage: www.elsevier.com/locate/jnucmat

Modeling copper precipitation hardening and embrittlement in a dilute Fe-0.3at.%Cu alloy under neutron irradiation

Xian-Ming Bai [a, c, *], Huibin Ke [b], Yongfeng Zhang [c], Benjamin W. Spencer [c]

[a] Department of Materials Science and Engineering, Virginia Polytechnic Institute and State University, Blacksburg, VA 24061, United States
[b] Department of Materials Science and Engineering, University of Wisconsin – Madison, Madison, WI 53706, United States
[c] Fuel Modeling and Simulation Department, Idaho National Laboratory, Idaho Falls, ID 83415, United States

ARTICLE INFO

Article history:
Received 24 May 2017
Received in revised form
10 August 2017
Accepted 25 August 2017
Available online 4 September 2017

Keywords:
Radiation hardening and embrittlement
Reactor pressure vessel steels
Cu precipitation in FeCu alloys
Cluster dynamics modeling

ABSTRACT

Neutron irradiation in light water reactors can induce precipitation of nanometer sized Cu clusters in reactor pressure vessel steels. The Cu precipitates impede dislocation gliding, leading to an increase in yield strength (hardening) and an upward shift of ductile-to-brittle transition temperature (embrittlement). In this work, cluster dynamics modeling is used to model the entire Cu precipitation process (nucleation, growth, and coarsening) in a Fe-0.3at.%Cu alloy under neutron irradiation at 300°C based on the homogenous nucleation mechanism. The evolution of the Cu cluster number density and mean radius predicted by the modeling agrees well with experimental data reported in literature for the same alloy under the same irradiation conditions. The predicted precipitation kinetics is used as input for a dispersed barrier hardening model to correlate the microstructural evolution with the radiation hardening and embrittlement in this alloy. The predicted radiation hardening agrees well with the mechanical test results in the literature. Limitations of the model and areas for future improvement are also discussed in this work.

1. Introduction

The reactor pressure vessel (RPV) is a safety-critical component in light water reactor nuclear power plants. It contains the reactor core and serves as a physical barrier to prevent the release of radioactive containments to the environment during severe accidents. Because of their massive size and location, RPVs are considered impractical to replace during a reactor's lifetime. In service, RPVs are exposed to long-term neutron irradiation at temperatures around 300°C [1]. For a 40-year service time, typically a RPV receives irradiation dose up to 0.1 displacement per atom (dpa) [1,2]. As for many other metals and alloys, irradiation can cause an increase of the yield strength (hardening) and a decrease of ductility and fracture toughness (embrittlement) in RPV steels [1,3]. Due to the radiation hardening and embrittlement, the ductile to brittle transition temperature (DBTT) shifts upward to a higher temperature upon long-term irradiation and thermal aging [1]. It has been shown that the shift in DBTT can be as large as 250°C under some circumstances [1,4], which could bring the DBTT close to the RPV operating temperature. Even much smaller DBTT shifts can lead to significant increases in the likelihood of a fracture initiating at the location of a pre-existing flaw in an RPV during a transient loading scenario. Therefore, predicting radiation-induced hardening and embrittlement is of significant interest when considering safety implications of long-term operation of current reactors.

RPVs are made of iron (Fe) based low-alloy ferritic steels, for which the composition varies slightly for reactors in different countries [1]. Minor elements, including manganese (Mn), nickel (Ni), silicon (Si), etc., as well as copper (Cu), are usually present in RPV steels, either as alloying elements or impurities. The concentration of these minor elements is typically less than 1 wt%. Although the concentration of minor elements is low, radiation can enhance or induce the precipitation of some alloy elements to form nano-size precipitates [2,5]. For example, Cu has a very low solubility in body-centered-cubic (bcc) iron. Even at the relatively high temperature of 700°C, the solubility limit is only about 0.5 wt% [6]. Neutron irradiation in reactors can accelerate the precipitation of Cu through the mechanism of radiation-enhanced precipitation.

* Corresponding author. Department of Materials Science and Engineering, Virginia Polytechnic Institute and State University, Blacksburg, VA 24061, United States.
E-mail address: xmbai@vt.edu (X.-M. Bai).

http://dx.doi.org/10.1016/j.jnucmat.2017.08.042
0022-3115/

Other precipitates have also been observed, such as Mn-Ni-Si clusters at high doses (the so-called "Late Blooming Phase") [5,7]. Although the average size of these clusters is only a few nanometers, they can serve as obstacles for dislocation motion. As a result, the yield strength increases and the failure strain decreases. In addition, irradiation creates dislocation loops and voids in the Fe matrix [1]. These microstructural features also contribute to radiation hardening and embrittlement.

The degradation of the mechanical properties of RPVs is directly related to reactor safety and is an important consideration for reactor lifetime extension. In the last few decades, radiation induced precipitation hardening and embrittlement has been an active research area in the nuclear materials field. Many experimental and modeling efforts have been conducted to investigate microstructural evolution and the change in mechanical properties in RPV steels as well as in model alloys. Experimentally, many studies have demonstrated that radiation induced embrittlement in RPV steels is very sensitive to the alloy composition [1]. For example, the increase in the concentration of Cu, Ni, and P leads to an increased susceptibility to embrittlement [1]. It has been shown more recently that Mn content also has a significant impact on embrittlement [8]. At the microstructural level, the properties of precipitates and other defects have been analyzed using a wide range of advanced characterization tools such as small angle neutron scattering (SANS) [9], atom probe tomography (APT) [10], positron annihilation spectroscopy (PAS) [11], and transmission electron microscopy (TEM) [12]. The comparison of these different characterization techniques on the same irradiation samples is summarized in Ref. [2]. Using these advanced microstructural characterization techniques, researchers have obtained valuable information about the composition, radius, number density, and volume fraction of the nanometer-size precipitates in RPV steels and model alloys [1,2]. The evolution of the precipitates strongly depends on alloy composition and irradiation conditions. Typically, the volume fraction of the precipitates increases with irradiation dose at low doses then reaches a saturated value at high doses [1]. It should be noted that each characterization technique has limitations, so using a combination of them can provide complementary results for the same sample [2]. In many studies, researchers have demonstrated that Cu-rich precipitates form in RPV steels and model alloys under neutron irradiation. It is commonly accepted that the precipitation of Cu-rich clusters plays an important role in causing radiation hardening and embrittlement in RPV steels. The Fe matrix may also form matrix defect features such as dislocation loops and microvoids [1]. Researchers [2,12] have shown that the number density of dislocation loops is about two orders of magnitude lower than that of Cu precipitates, while the number density of vacancy-type clusters is slightly higher than that of Cu precipitates in Fe-0.1at.%Cu and Fe-0.3at.%Cu model alloys. Lambrecht et al. [13] used a theoretical model to estimate the contribution to radiation hardening from Cu precipitates and matrix defects in these alloys. Their conclusion is that although dislocation loops are stronger obstacles than precipitates for dislocation motion, the contribution from dislocation loops to the hardening is small due to their low number density. Vacancy-type clusters or microvoids are considered to have no contribution to radiation hardening due to their small sizes [13]. The precipitation of other types of clusters such as Mn-Ni-Si clusters at high doses may affect the mechanical properties of RPV steels significantly, and this is a topic of active research [7,8]. To represent the effect of irradiation on material properties for engineering analyses, models [1] such as the EONY model [4,8] have been developed to describe the DBTT shift as a function of irradiation doses for RPV steels of different compositions. The parameters in these models are empirically fitted to the database obtained from a large number of the surveillance samples.

Although the engineering models mentioned above are very powerful for predicting the radiation embrittlement of RPV steels, their representation of microstructural evolution is either lacking or based on empirical data rather than physics-based models. Likewise, they employ empirical correlations between microstructure and mechanical properties. In addition, the flux effect [14] is not well addressed in these models, which can be a challenge for extrapolating the results of accelerated irradiation tests to realistic RPV irradiation conditions. Furthermore, the models only can be applied to RPV steels of specific composition ranges [1]. Since the microstructural evolution governs the degradation of the mechanical properties in irradiated RPV steels, mesoscale modeling methods such as atomic kinetic Monte Carlo (AKMC) [15–17] and cluster dynamics [18,19] have been applied to study the Cu precipitation in bcc iron under both irradiation and thermal aging conditions. Becquart and Wirth [16] have used AKMC to model Cu precipitation in a Fe-0.3%Cu at dose rates comparable to those experienced by RPV steels in reactors. The cascade-induced defects were introduced into the simulation systems at certain time intervals based on dose rates. One major conclusion from this work is that the decrease in dose rate enhances Cu precipitation. AKMC has also been used to study the Cu precipitation in high-Cu Fe-Cu alloys, taking into account the effects of mobile Cu clusters [17]. Although AKMC has spatial resolution and can capture some atomic details of the precipitation process, the computational cost is relatively expensive. An alternative approach is rate theory based cluster dynamics modeling [20]. Cluster dynamics is a mean-field approach in which the clusters and defect sinks are assumed to be homogenously distributed in the system. It can model the nucleation, growth, and coarsening of the precipitates in the same framework. The evolution of point defects, which is directly related to radiation-enhanced diffusion of solute atoms, can be naturally coupled to the precipitation model. This method has been successfully applied to model Cu precipitation under electron and neutron irradiation conditions in some high-Cu alloys such as Fe-1.34at.%Cu [18] and the predicted precipitation kinetics has good agreement with experimental measurement. In addition to modeling solute precipitation under irradiation [18] and thermal aging [19], this method has also been extensively applied to model the evolution of dislocation loops and voids in pure metals [21–23].

The Cu concentration in realistic RPV steels is very low, typically below 0.1 at.% [1]. In this work, we use cluster dynamics modeling to model the Cu precipitation under neutron irradiation conditions at 300°C in a Fe-0.3 at.%Cu alloy, which is much closer to the Cu concentration in realistic RPV steels than the previously studied Fe-1.34 at.%Cu alloys [18]. Similar to the Fe-1.34 at.%Cu work, a homogenous precipitation mechanism is assumed so that this work will demonstrate whether such a mechanism can still be assumed for Cu precipitation in the Fe-0.3 at.%Cu alloy, which has not been done previously. Note that previously cluster dynamics modeling [24] has shown that the homogenous precipitation mechanism may not be assumed for Cu concentration lower than 0.1 wt% (0.088 at.%) in Fe. Instead the heterogeneous precipitation of Cu-rich clusters at point defect clusters is likely to dominate the process. To our best knowledge, a quantitative heterogeneous precipitation model for low-Cu (<0.1 wt%) alloys still does not exit. Development of such a heterogeneous precipitation model (or a homogenous precipitation model within a different parameter set) for low-Cu alloys is beyond the scope of this work but can be a future research topic. To connect the microstructural evolution with the mechanical properties, a size-dependent dispersed barrier hardening model is used to correlate the precipitate size distribution with the radiation hardening and embrittlement. Experimental results for both Cu precipitation kinetics [2,9] and radiation

hardening [11,13] are available for this alloy in literature, and are used to calibrate our model. Through the combination of cluster dynamics modeling and a dispersed barrier hardening model, the evolution of radiation hardening and DBTT shift as a function of irradiation dose is predicted in this work for the Fe-0.3 at.%Cu alloy.

The paper is organized as follows. In Section 2, results from the cluster dynamics model for Cu precipitation under electron irradiation in a Fe-1.34 at.%Cu [18] are reproduced to ensure the correct implementation of the modeling framework. In Section 3, this cluster dynamics model is modified to model Cu precipitation in a Fe-0.3 at.%Cu alloy under neutron irradiation and the results are compared with experiments. In Section 4, a size-dependent dispersed barrier hardening model and a superposition law are used to connect the microstructural evolution with the radiation hardening. In addition, the evolution of DBTT shift as a function of irradiation dose is also predicted based on a correlation between hardening and DBTT shift. Finally discussion and conclusions are presented.

2. Cluster dynamics modeling of Cu precipitation in Fe-1.34 at.%Cu under electron irradiation

Cluster dynamics has been used to model Cu precipitation in bcc Fe under both irradiation [18] and thermal aging [19] conditions. When Cu clusters are small, they have the same bcc crystal structure as the Fe matrix so that the interface between bcc Cu precipitates and Fe matrix is coherent. When the precipitates grow to a certain size (e.g., 2–3 nm in radius), the bcc structure transforms to a twinned 9R structure [25–27]. As the precipitate radius grows to about 6–10 nm, the crystal structure transforms to a stable face-centered-cubic (fcc) structure [25]. In this work, only the coherent bcc Cu precipitates are modeled because the mean precipitate radius reaches about 2 nm in the dilute Fe-0.3 at.%Cu alloys in experiments [2,13]. In previous AKMC modeling, more realistic vacancy formation and migration energies calculated from density functional theory (DFT) were used and small Cu clusters were also considered to be mobile [17]. In our work the defect energies and other parameters are similar to Ref. [18] because we would like to adapt this validated model as the first step. In addition, only Cu monomers are considered diffusing for simplicity, which is the same assumption made in Ref. [18]. Note that the Cu monomer diffusivity in cluster dynamics modeling [18] is about 1000 times higher than that used in AKMC simulation [17] while both methods can reproduce the experimental Cu precipitation kinetics. As the authors of Ref. [17] argued, the reason is that "the overestimation of the copper diffusion coefficient compensates the absence of cluster migration". In other words, the contribution of Cu diffusivity from mobile Cu clusters can be effectively included in the overestimated Cu monomer diffusivity if only Cu monomers are assumed to be mobile.

In this section, the previously published cluster dynamics model for Cu precipitation in a Fe-1.34at.%Cu under electron irradiation [18] is reproduced first to ensure that our cluster dynamics modeling framework works appropriately. Some parameters from this high-Cu model will be adapted to study the Cu precipitation in a dilute Fe-0.3at.%Cu under neutron irradiation, as discussed in the next section. Although the model was described in several references [18,19,28], in this manuscript we provide the full details of the model to present this approach in a self-contained manner so that other researchers can reproduce this work conveniently. In cluster dynamics modeling, the size of each class of cluster can be represented by the number of atoms it contains. Each class of cluster has a concentration based on the mean field assumption. The concentration of a cluster containing n Cu atoms is represented by C_n. Since only Cu monomers are considered mobile in this work, Cu clusters only interact with single Cu atoms (monomers). When a cluster of size n absorbs one Cu monomer, its size become $n+1$. When a cluster of size $n+1$ emits one Cu monomer through thermal emission, its size decreases to n. Therefore, the flux from cluster size n to $n+1$ is:

$$J_{n\to n+1} = \beta_n C_1 C_n - \alpha_{n+1} C_{n+1}, \tag{1}$$

where β_n is the absorption coefficient for a cluster of size n and α_{n+1} is the emission coefficient for a cluster of size $n+1$. Assuming all clusters (including monomer) have a spherical geometry, the radius of a cluster of size n is $r_n = \left(\frac{3nV_{at}}{4\pi}\right)^{1/3}$, where $V_{at} = a_0^3/2$ is the volume per bcc Cu atom and a_0 is the lattice parameter for bcc Fe. The absorption coefficient β_n is related to the radius of a Cu monomer (r_1), the radius of the Cu cluster of size n (r_n), the Cu diffusion coefficient in Fe matrix (D_{Cu}), and the atomic volume of a bcc Cu atom (V_{at}),

$$\beta_n = \frac{4\pi(r_1 + r_n)D_{Cu}}{V_{at}}. \tag{2}$$

The emission and absorption coefficients are exponentially related by the binding energy of the Cu cluster (E^b), the Boltzmann constant (k_B), and the temperature (T):

$$\alpha_{n+1} = \beta_n \exp\left(-\frac{E^b_{n+1}}{k_B T}\right). \tag{3}$$

In Eq. (3), the cluster binding energy E^b is size-dependent and related to the cluster interface energy σ. The binding energy for a cluster size of $n+1$ is

$$E^b_{n+1} = \Omega - T\cdot\Delta S - (36\pi)^{1/3}\cdot V_{at}^{2/3}\cdot\sigma\cdot\left[(n+1)^{2/3} - n^{2/3}\right], \tag{4}$$

where Ω is enthalpy change for dissolving Cu in Fe and ΔS is non-configurational entropy [18], respectively. So $G_1 = \Omega - T\Delta S$ is the Gibbs free energy change for the mixing, which determines the solubility of Cu monomer in Fe at a temperature T:

$$C_{eq}(T) = \exp\left(-\frac{\Omega - T\Delta S}{k_B T}\right). \tag{5}$$

Here $\Omega/k_B = 6255$ K and $\Delta S = 0.866\ k_B$ are used [18], which give the Cu solubility of $C_{eq} = 4.3\times10^{-5}$ at 300°C (573 K). Eq. (4) can also be viewed as the energy gain associated with attaching a monomer to a cluster of size n, or $E^b_{n+1} = G_1 + G_n - G_{n+1}$, which is the definition of the binding energy for a cluster of size $n+1$. The interfacial energy is usually treated as a fitting parameter in cluster dynamics modeling [19,28]. For Cu precipitation in Fe, the value is in the range between 0.15 and 0.5 J/m^2 for a coherent interface [25]. In some work the interface energy has been treated as both size and temperature dependent [19]. In Ref. [18], the interface energy was not explicitly provided. In our work the interface energy is set to 0.37 J/m^2 regardless of cluster size and temperature. Using Eq. (4), the size-dependent binding energy can be obtained, as shown in Fig. 1. The binding energy increases with the increasing cluster size and gradually approaches a saturated value. Fig. 1 is very similar to the plot of size-dependent binding energy in Ref. [18], indicating that 0.37 J/m^2 is the right value for the interfacial energy.

Since Cu clusters can either grow or shrink, the concentration of each cluster size (C_n) evolves dynamically with time. Each cluster size can evolve to one of its two neighboring cluster sizes through either absorbing or emitting a monomer. Therefore, the time evolution of C_n is related to the fluxes from or to its two neighboring

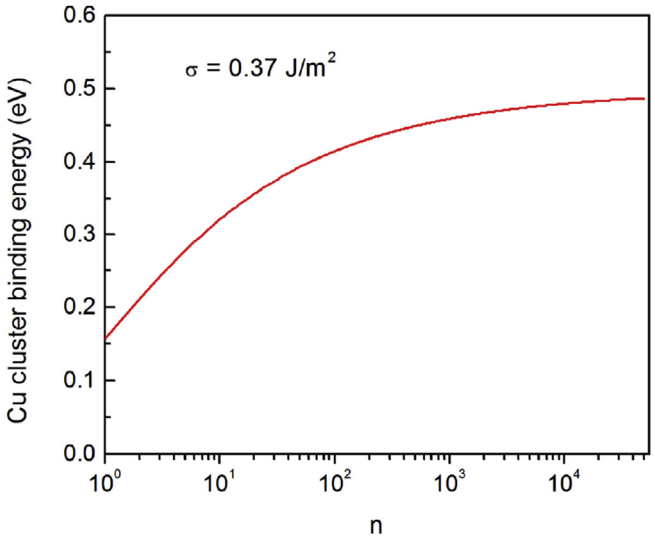

Fig. 1. Size dependence of Cu cluster binding energy.

sizes,

$$\frac{dC_n}{dt} = J_{n-1\to n} - J_{n\to n+1}, \quad (n \geq 2). \tag{6}$$

Note that Eq. (6) is valid only if $n \geq 2$ because the flux $J_{0\to 1}$ does not exist. For the evolution of the concentration of the monomer (C_1), the situation is more complex. For all $n \geq 2$ fluxes $J_{n\to n+1}$, one Cu monomer is involved through either absorption or emission processes. Therefore, the evolution of C_1 is related to all these $n \geq 2$ fluxes. For the flux $J_{1\to 2}$, two Cu monomers are needed to form a di-Cu cluster during the absorption process. Similarly, a di-Cu cluster splits into two Cu monomers during the emission process. So the contribution from the $J_{1\to 2}$ flux to the evolution of C_1 should be doubled. Overall, the time evolution of C_1 can be represented as:

$$\frac{dC_1}{dt} = -2J_{1\to 2} - \sum_{n\geq 2}^{\infty} J_{n\to n+1}. \tag{7}$$

Eqs. (6) and (7) describe the time evolution of all cluster sizes ($n = 1 - \infty$). Practically, a maximum cluster size n_{max} is used and its flux is set to zero as the boundary condition. The n_{max} should be sufficiently large so that its concentration is close to zero during the simulation. Solving the n_{max} ordinary differential equations, the concentration of each cluster size can be obtained as a function of time. Thus the cluster size distribution (i.e., C_n vs. n) also can be obtained at any given time.

Since Cu atoms form substitutional atoms in bcc Fe, the Cu diffusion in Fe is mediated by vacancies during thermal aging. Under irradiation, Cu might also diffuse via the interstitial mechanism. However, Christien and Barbu [18] argued that the contribution from interstitial-mediated Cu diffusion is negligible. Therefore, only the vacancy-mediated Cu diffusion mechanism is considered in this work. For thermal aging, the thermal vacancy concentration determines the Cu diffusivity. Under irradiation, vacancies are produced directly by energetic particles so that the vacancy concentration can be much higher than the thermal vacancy concentration, particularly at low and moderate temperatures. As a result, Cu diffusion under irradiation is enhanced significantly by irradiation. The radiation enhanced Cu diffusivity is described by

$$D_{Cu}^{irr} = D_{Cu}^{th}\frac{C_v^{irr}}{C_v^{th}}, \tag{8}$$

where the superscripts *th* and *irr* represent the thermal and irradiation conditions, respectively, for vacancy concentration (C_v) and Cu diffusion coefficient (D_{Cu}). The ratio of C_v^{irr}/C_v^{th} is the radiation-enhanced factor for Cu diffusion. The temperature-dependent thermal diffusion coefficient of Cu can be described by $D_{Cu}^{th} = D_{Cu}^{0}\cdot\exp(-E_{Cu}^{m}/k_BT)$, where D_{Cu}^{0} and E_{Cu}^{m} are the prefactor and activation energy of Cu diffusion in bcc Fe, respectively. The thermal vacancy concentration is related to the vacancy formation energy (E_v^f) in Fe and to the temperature by $C_v^{th} = \exp(-E_v^f/k_BT)$. Same as in Ref. [18], $E_v^f = 1.6$ eV is used. The vacancy concentration under irradiation (C_v^{irr}) depends on defect production rate, defect reaction and defect loss to sinks. As in Ref. [18], here a simplified rate theory model is used to describe the point defect evolution under irradiation. In this model, only defect production, defect recombination, and defect loss to dislocations are considered. For simplicity, defect clustering and other defect sinks are not considered. The time evolution of vacancy concentration (C_v) and interstitial concentration (C_i) are described by the following two rate equations [18],

$$\frac{dC_v}{dt} = \varepsilon G_0 - k_{iv}C_iC_v - z_vD_vC_v\rho_d, \tag{9}$$

$$\frac{dC_i}{dt} = \varepsilon G_0 - k_{iv}C_iC_v - z_iD_iC_i\rho_d, \tag{10}$$

where ε is cascade efficiency; G_0 is defect production rate or irradiation dose rate; k_{iv} is defect recombination coefficient between interstitials and vacancies; $D_v = D_v^0\cdot\exp(-E_v^m/k_BT)$ is temperature-dependent Fe vacancy diffusion coefficient, where D_v^0 and E_v^m are the prefactor and migration energy for vacancy diffusion, respectively; Similarly, $D_i = D_i^0\cdot\exp(-E_i^m/k_BT)$ is temperature-dependent Fe interstitial diffusion coefficient, where D_i^0 and E_i^m are the prefactor and migration energy for interstitial diffusion, respectively; ρ_d is dislocation density; and $z_i = 1.2$ and $z_v = 1.0$ are the absorption efficiencies for interstitials and vacancies, respectively. Typically it is assumed $z_i > z_v$ so that a dislocation absorbs more interstitials than vacancies (the so-called "dislocation bias") [20]. By solving Eqs. (9) and (10), the time evolution of vacancies and interstitials under irradiation can be obtained. This then permits the calculation of radiation enhanced Cu diffusion using Eq. (8).

The cluster dynamics model coupled with radiation-enhanced diffusion model is first used in this study to simulate the precipitation of Cu clusters in a Fe-1.34 at.%Cu alloy under electron irradiation at 290°C with a dose rate of 2×10^{-9} dpa/s, using the same parameters as in Ref. [18]. These parameters are summarized in Table 1. Since electron irradiation only produces Frenkel pairs, the cascade efficiency is $\varepsilon = 1.0$. The dislocation density in the simulation is $\rho_d = 10^{12}$ m^{-2}. The Fe interstitial and vacancy migration barriers are 0.3 eV and 1.3 eV, respectively. Note that this interstitial migration barrier is close to the atomistic calculation results, but the vacancy migration barrier is about twice of atomistic calculation results for pure Fe [29]. The discrepancy may be attributed to solute or impurity drag effects in realistic alloys. The use of these values in Ref. [18] has resulted in good agreement with experimentally measured precipitation kinetics. Therefore, these migration barriers are used in this study. At the steady state of point defect evolution, the radiation-enhanced factor for Cu diffusion is about 2.5×10^7 so that the Cu precipitation kinetics is enhanced significantly by the irradiation. In Ref. [18], Eqs. (9) and (10) were calculated separately from the cluster dynamics modeling and only the steady state value of the radiation-enhanced diffusion factor

Table 1
Parameters for cluster dynamics modeling of Cu precipitation in a Fe-1.34at.%Cu alloy under electron irradiation at 290°C. The parameters are taken from Ref. [18].

Parameter	Value
C_1^0, initial Cu concentration	1.34 at.%
a_0, lattice constant of bcc Fe	2.867 Å
T, temperature	563 K (290°C)
E_{Cu}^m, activation energy of Cu thermal diffusion in Fe	2.29 eV
D_{Cu}^0, prefactor of Cu thermal diffusion in Fe	6.3×10^{-5} m^2/s
Ω, heat of mixing of Cu in Fe	6255 $k_B \cdot K$
ΔS, non-configurational entropy	$0.866 \cdot k_B$
σ, interface energy for coherent Cu-Fe interface	0.37 (J/m^2)
G_0, defect production rate	2×10^{-9} dpa/s
ε, cascade efficiency	1.0
ρ_d, dislocation density	1.0×10^{12} m^{-2}
E_i^m, Fe interstitial migration energy	0.3 eV
D_i^0, prefactor of Fe interstitial diffusion	4.0×10^{-8} m^2/s
E_v^m, Fe vacancy migration energy	1.3 eV
D_v^0, prefactor of Fe vacancy diffusion	1.0×10^{-4} m^2/s
r_{iv}, defect recombination radius	6.5 Å
z_i, dislocation absorption efficiency for interstitials	1.2
z_v, dislocation absorption efficiency for vacancies	1.0
E_v^f, vacancy formation energy in Fe	1.6 eV

was used. In our work, Eqs. (9) and (10) are directly coupled to the cluster dynamics modeling [Eqs. (6) and (7)] so that the radiation-enhanced Cu diffusion evolves dynamically during the Cu precipitation process. The direct coupling results in slower precipitation in the nucleation and growth stage than using the steady-state value. But the coarsening stage (where the experimental validation is made) is not affected.

The coupled cluster dynamics and rate theory equations ([Eqs. (6-7) and (9-10)]) are solved using the CVODE solver of SUNDIALS package [30]. The Backward Differentiation Formulas (BDF) implicit method is used to integrate the differential equations and Newton method is used for the iteration. At each time step the solver needs to solve n_{max}+2 coupled ordinary differential equations, where n_{max} is the total number of cluster classes and 2 represents the two point defect evolution equations. As mentioned earlier, the maximum cluster size n_{max} should be large enough so that its concentration is close to zero during the entire simulation. However, the computational cost is high when n_{max} is large. To improve the computational efficiency, a few approaches are used. First, a banded linear solver (CVBAND) is used. In this work, only Cu monomers are diffusing. Therefore, for all cluster sizes greater than or equal to 2, C_n only couples with its two neighboring cluster sizes and C_1. As a result, the Jacobian matrix is a banded matrix. The banded linear solver is used to take advantage of this sparse matrix feature. Second, the grouping method developed by Golubov et al. [31] is implemented into our cluster dynamics code. The basic idea of the grouping method is to group clusters into different groups based on their sizes. If the group size is chosen appropriately, the cluster concentration within each group has an approximately linear correlation with the cluster size. Using this method, only two differential equations are solved for each group. The concentration of each cluster size can then be linearly extrapolated based on the solutions of the two differential equations for a given group. Using the grouping method, the number of differential equations to be solved can be reduced significantly, with a corresponding improvement in efficiency. To demonstrate that the grouping method works correctly, a test with parameters listed in Table 1 is conducted. In this test, n_{max} = 50,000 and Cu cluster evolution is computed over 50,000 s. For the first 100 cluster sizes, each class of cluster has a group size of 1. For n > 100 cluster sizes, the clusters are put into 231 groups so that in total, 331 groups are created. Fig. 2(a) compares the evolution of the total Cu cluster number density between the standard cluster dynamics simulation (no grouping) and the grouping method. Here the number density is the number of clusters per unit volume. It can be converted from the cluster concentration by

$$N_n = C_n / V_{at}. \tag{11}$$

In experimental characterization techniques such as small angle neutron scattering (SANS), the detection limit is about 0.5 nm in terms of radius [2,9]. Using the same definition as in Ref. [18], only clusters containing more than 10 Cu atoms (equivalent to the cluster radius of 0.3 nm) are included in the total cluster number density calculation in Fig. 2(a). Note that this threshold value is slightly smaller than the detection limit in SANS experiments. However, in the next section it will be shown that using the same threshold as in experiments does not affect the results in the coarsening regime, where experimental validations are typically made. Clearly, the grouping method produces results identical to those from the standard method over the entire time range, indicating that the grouping method has been correctly implemented. Fig. 2(b) compares the computational times of the two simulations. Using the grouping method, the computational time is reduced by 300 times. In other cases, the computational time has been reduced by up to 400 times.

The maximum cluster size (n_{max} = 50,000) used in Fig. 2 is for demonstration purposes only. If the simulation time is long, it was found that this maximum cluster size is not sufficient for studying the Cu precipitation in the Fe-1.34Cu at.% alloy under electron irradiation. Therefore, for the other simulations presented here, a larger maximum cluster size of n_{max} = 200,000 is used for this alloy. Using the grouping method, 870 groups are created (including the first 100 groups with group size of 1). Precipitate evolution is evaluated over about 2×10^6 s. The solid line in Fig. 3(a) shows the time evolution of the total number density of Cu clusters that contain more than 10 Cu atoms (n > 10). The corresponding irradiation dose is also shown in the top horizontal axis. Similarly, the solid line in Fig. 3(b) shows the time evolution of the mean radius of all the clusters having n > 10 Cu atoms. The mean radius is calculated by

$$\bar{r} = \frac{\sum_{n=11}^{n_{max}} (r_n \cdot C_n)}{\sum_{n=11}^{n_{max}} C_n}. \tag{12}$$

As Fig. 3(a) shows, initially the total cluster number density increases rapidly with the irradiation time or dose. Then the number density reaches a maximum value of about 4.5×10^{25} m^{-3} at about 30 s. Meanwhile, the mean cluster radius remains nearly constant (Fig. 3(b)). This behavior indicates that the cluster nucleation and growth dominate this stage through depleting the Cu monomers in the Fe matrix. Next the cluster number density decreases but the mean radius increases rapidly. This behavior indicates that the Ostwald ripening induced cluster coarsening dominates the cluster evolution in this regime.

The dose-dependent cluster number densities and mean radii measured from SANS experiments [28] for the same alloy composition under the same electron irradiation conditions are shown as open circles in Fig. 3 for validating the precipitation model. It can be seen that the modeling results agree reasonably well with the SANS experimental results in the coarsening regime for both the total number density of Cu clusters and the mean cluster radius. The results also agree well with published results from the referenced model, indicating that it has been successfully reproduced and the code works correctly.

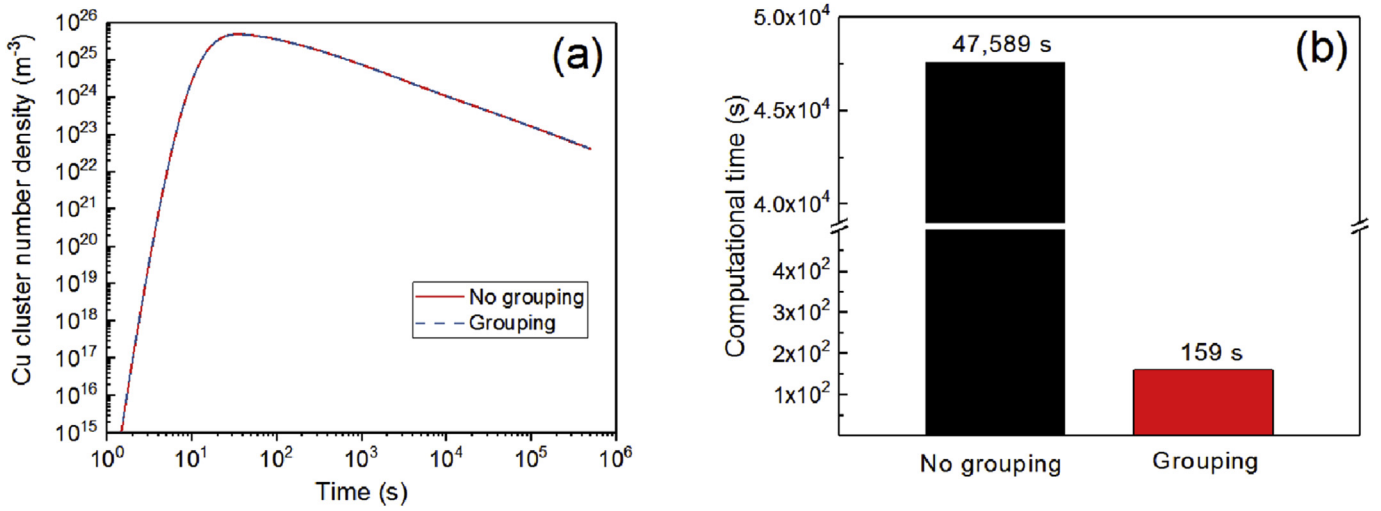

Fig. 2. Comparison of cluster dynamics simulations with and without using the grouping method. (a) The time evolution of the Cu cluster number density. The simulation using grouping method produces results identical to those without using the grouping method. (b) The computational times of the two simulations. The computational time is reduced about 300 times by using the grouping method.

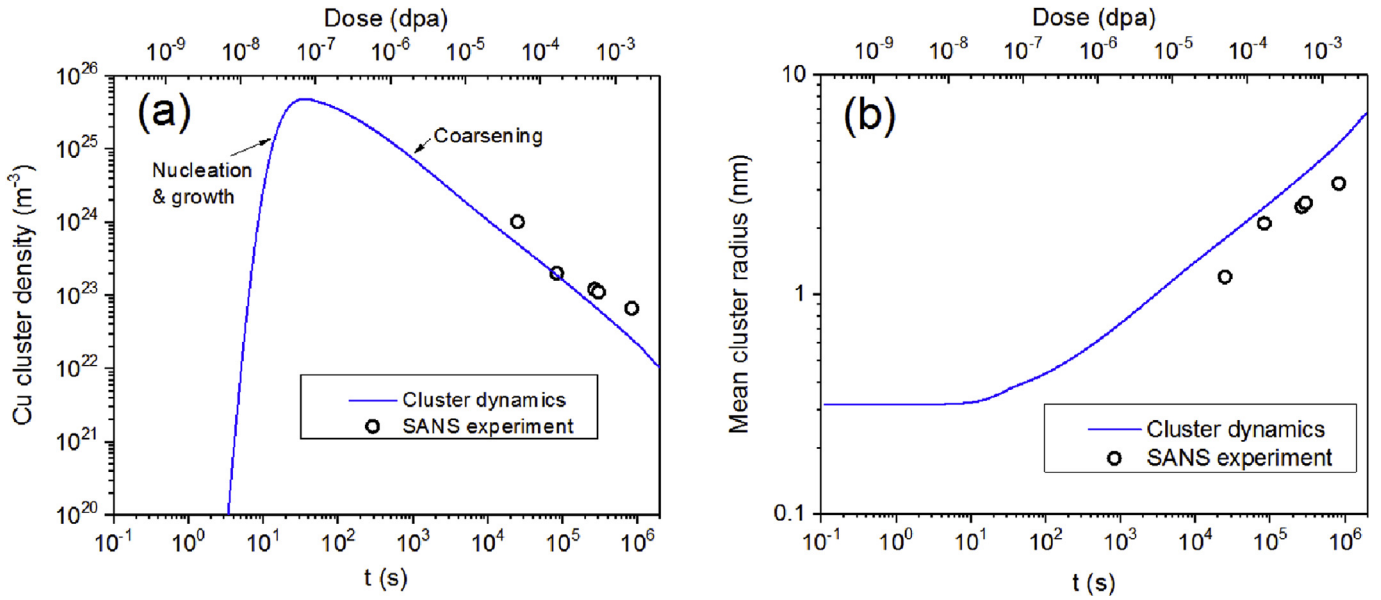

Fig. 3. Cluster dynamics modeling of electron-radiation-enhanced precipitation of Cu clusters in a Fe-1.34 at.%Cu at 290°C based on Ref. [18]. The modeling results (lines) are validated by the small-angle neutron scattering (SANS) experiments (open circles). (a) Evolution of Cu cluster number density as a function of irradiation time or dose. (b) Evolution of the mean Cu cluster radius as a function of irradiation time or dose. Note that in both figures only clusters containing more than 10 Cu atoms are counted.

3. Cluster dynamics model for Cu precipitation in Fe-0.3 at.% Cu under neutron irradiation

In the electron irradiation experiment for the Fe-1.34at.%Cu alloy [28], the Cu concentration is much higher than that in realistic RPV steels, which is typically below 0.1 at.% [1]. Recently, researchers [2,9] characterized the Cu precipitation in Fe-based alloys containing both 0.1 at.% and 0.3 at.% of Cu under neutron irradiation at 300°C. While it is desired to model the Cu precipitation in both alloys, modeling Cu precipitation in the Fe-0.1 at.%Cu may require the assumption of a heterogeneous precipitation mechanism [24] but such a quantitative model has not been well established to our best of knowledge. Thus, as a first step we focus on the precipitation in the Fe-0.3 at.%Cu alloy based on the assumption of homogenous precipitation. This 0.3 at.% Cu concentration is still a little higher than that in realistic RPV steels, but it is much closer than the Fe-1.34Cu at.% alloy. Modeling Cu precipitation in the Fe-0.1 at.%Cu alloy through either a heterogeneous or a homogenous precipitation model with different model calibration will be a future research topic. In Meslin et al.'s work [2], the neutron irradiation dose rate is about 1.4×10^{-7} dpa/s and the dislocation density in the alloy is about $\rho_d = 5 \times 10^{13}$ m^{-2}. Therefore both the irradiation conditions and material properties are quite different from those in the electron irradiation.

To test the transferability of the model discussed in Section 2, the same parameters listed in Table 1 (which are for the Fe-1.34Cu at.% alloy under electron irradiation) are first used, except that the material properties (Cu concentration, dislocation density) and irradiation conditions (dose rate, irradiation temperature) are changed to those in the Fe-0.3Cu at.% alloy experiment. The

maximum cluster size is 50,000 for this alloy. Under the new irradiation conditions, the radiation enhanced diffusion factor is 9.1×10^7 at the steady state based on Eqs. (9) and (10). The evolution of the total Cu cluster number density and the evolution of mean Cu cluster radius are shown as the dashed lines in Fig. 4(a) and (b), respectively. Same as in Section 2, only Cu clusters containing more than 10 Cu atoms are counted in Fig. 4. The results determined by the SANS experiments [2,9] are shown as the filled circles in each figure. The model as described in Section 2 predicts lower number density and larger mean radius compared with the experimental results. In other words, the predicted precipitation kinetics from the model is much faster than that in the neutron irradiation experiments. This discrepancy suggests that this model cannot be directly used when the material properties and irradiation conditions change. Therefore, some adjustment of the input parameters is needed.

Although it is very common to adjust the input parameters in cluster dynamics modeling when the material properties and irradiation conditions change, it is desirable to have a model that can predict a variety of conditions with minimal parameter adjustment. In addition, there must be reasonable justification for any adjustment. Here only two parameters are adjusted: the cascade efficiency (ε) and the vacancy migration energy (E_v^m). In the model in Section 2, these two parameters have the values: $\varepsilon = 1$ and $E_v^m = 1.3$ eV. Recall that that model is for electron irradiation. In electron irradiation, only Frenkel pairs are produced so that defect production efficiency is high ($\varepsilon = 1$). In the Fe-0.3Cu at.% alloy studied here, the Cu precipitation is under neutron irradiation. It is well known that neutron irradiation produces dense collision cascades in which many displaced atoms can have in-cascade recombination. Thus, the defect production efficiency in neutron irradiation is lower than electron irradiation [32]. Similar to the value suggested by Stoller et al. [22], here the cascade efficiency is set to $\varepsilon = 0.4$ to capture the in-cascade recombination effects during neutron irradiation. Using this cascade efficiency, the new results are shown in dotted lines in both figures in Fig. 4. However, this adjustment only slightly improves the agreement of the predicted precipitation kinetics with the experimental results. Note that in neutron irradiation, defect clusters can be directly produced in cascades. Therefore, modeling the effects of defect clustering on solute precipitation requires more sophisticated models. Previous work [18] has shown that the incorporation of such models sometimes does not affect the precipitation kinetics in the coarsening regime while sometimes it is critical for predicting the right precipitation kinetics. In this work, the defect clustering is not included in our model for simplicity. It will be shown below that this simple model still works well through a proper calibration.

Next the vacancy migration energy (E_v^m) is changed from 1.3 eV to 1.0 eV based on the solute drag effect. In alloys, solute elements can interact with point defects and cause solute trapping effects on point defect diffusion. It has been found that Cu atoms and clusters can trap vacancies in Fe [17]. Since in the neutron irradiation experiment the Cu concentration is much lower than in the electron irradiation experiment (0.3 vs. 1.34 at.%), it is reasonable to assume that the effect of solute trapping on vacancy diffusion is weaker in the low-Cu alloy (this work) than in the high-Cu alloy (original model). Therefore, the decrease of the vacancy migration energy from 1.3 eV to 1.0 eV has a reasonable justification although the magnitude of the decrease is empirically chosen. Note that in previous cluster dynamics modeling researchers had increased the vacancy migration energy for more complex alloys based on a solute trapping mechanism in order to reproduce the experimental data [33]. Our approach is similar because we decrease the vacancy migration energy when the alloy is less complex. The adjustment of vacancy migration energy may affect Cu thermal diffusivity. Here the assumption is that this adjustment only affects the vacancy concentration under irradiation and thus the radiation-enhanced diffusion. Table 2 summarizes the parameters that are different from those in Table 1. Note that the material properties and irradiation conditions listed in Table 2 are not adjustable parameters because they need be consistent with the new experiment.

Using the new cascade efficiency ($\varepsilon = 0.4$) and vacancy migration energy ($E_v^m = 1.0$ eV), the radiation enhanced Cu diffusion factor decreases from 9.1×10^7 to about 7.7×10^5 at the steady state based on Eqs. (9) and (10). This decrease of Cu diffusion leads to slower coarsening kinetics. The solid lines in Fig. 4(a) and (b) show

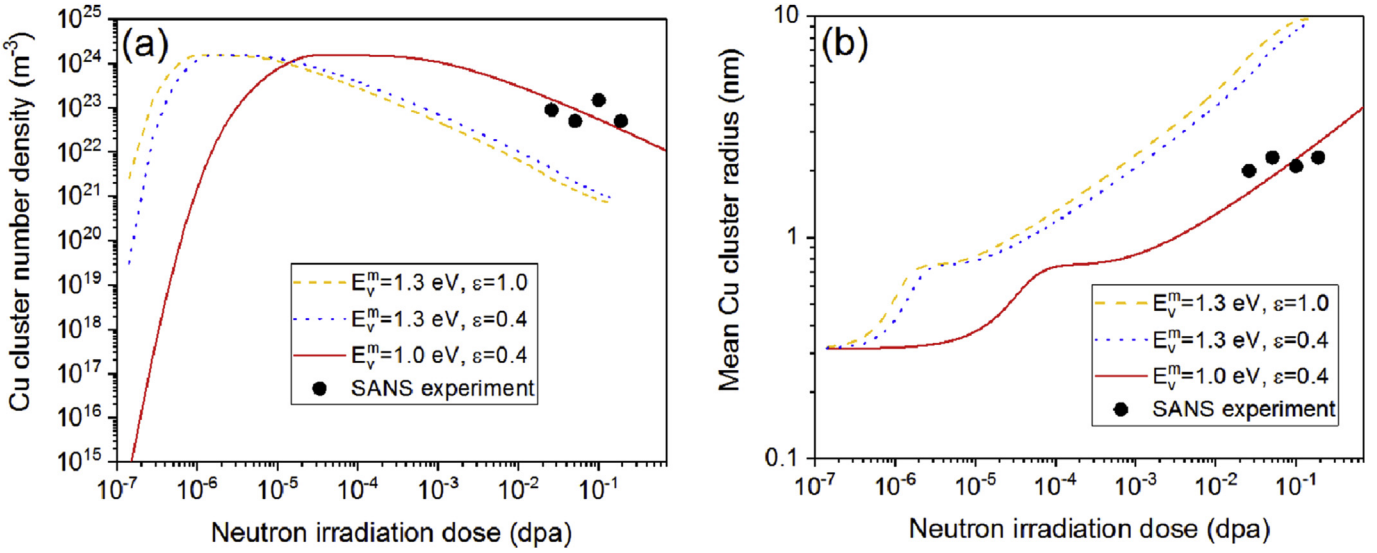

Fig. 4. Cluster dynamics modeling results for neutron-radiation-enhanced precipitation of Cu clusters in a Fe-0.3 at.%Cu at 300°C using three sets of parameters. (a) Evolution of Cu cluster number density as a function of irradiation dose. (b) The evolution of the mean Cu cluster radius as a function of irradiation dose. Note that in both figures only clusters containing more than 10 Cu atoms are counted. In both figures, the dashed lines represent the modeling results using the cascade efficiency ($\varepsilon = 1.0$) and vacancy migration energy ($E_v^m = 1.3$ eV) of the model in Ref. [18]. The dotted lines are from changing just the cascade efficiency ($\varepsilon = 0.4$, $E_v^m = 1.3$ eV). The solid lines represent the final model using two modified parameters ($\varepsilon = 0.4$, $E_v^m = 1.0$ eV). The results from small-angle neutron scattering experiments (solid circles) [2,9] are shown for validation.

Table 2
Comparison of the parameters for modeling Cu precipitation in the Fe-1.34at.%Cu and Fe-0.3at.%Cu alloys. Other parameters are as same as in Table 1.

	Original model [18]	This work
Materials properties		
C_i^0, initial Cu concentration	1.34 at.%	0.3 at.%
ρ_d, dislocation density	1.0×10^{12} m^{-2}	5×10^{13} m^{-2}
Irradiation conditions		
Irradiation particles	Electron	Neutron
T, temperature	563 K (290°C)	573 K (300°C)
G_0, defect production rate	2×10^{-9} dpa/s	1.4×10^{-7} dpa/s
Adjusted parameters		
ε, cascade efficiency	1.0	0.4
E_v^m, Fe vacancy migration energy	1.3 eV	1.0 eV

the new cluster dynamics predictions using the new parameter set. The modeling results agree with experimental SANS measurement [2,9] very well for both cluster number density and mean radius. Compared to the Fe-1.34 at.%Cu alloy under the electron irradiation, the maximum cluster number density is about 20–30 times lower because the Cu concentration in the Fe-0.3 at.%Cu alloy is much lower. The cluster coarsening also happens at a much higher dose range than in the electron irradiation. The mean Cu cluster radius is much smaller for the full range of irradiation doses considered here.

Using the new parameter set ($\varepsilon = 0.4$, $E_v^m = 1.0$ eV) the coarsening kinetics is slower than the original parameter set ($\varepsilon = 1.0$, $E_v^m = 1.3$ eV). To explain the reason, the evolution of the point defect concentration for the two parameter sets is shown in Fig. 5, which is calculated from Eqs. (9) and (10). It can be seen that the resulting vacancy concentration is lower when the vacancy migration energy is lower. When the vacancy migration energy is higher (1.3 eV), vacancies are less mobile. Therefore vacancies keep buildup while interstitials are annihilated by sinks. Later vacancies also can be annihilated by sinks so that the steady state is reached. When the vacancy migration energy is lower (1.0 eV), vacancies are more mobile. Therefore vacancies can find sinks at a much earlier time than the case of slower vacancy diffusion. As a result, the steady state is reached at a much earlier time and the vacancy buildup (concentration) is also much lower. In turn, the radiation-enhanced Cu diffusion, which is proportional to the vacancy concentration (Eq. (8)), is slower when the vacancy migration energy is lower.

At any given irradiation dose (or time), the size distribution of Cu clusters, which is the number density of each class of cluster versus the cluster radius, also can be obtained in addition to the evolution of the total number density and mean cluster radius previously shown. Fig. 6 shows the cluster size distribution at 0.14 dpa, which is slightly higher than the upper limit of the total dose received in RPV steels over 40 years [13]. For small clusters ($r < 0.25$ nm or $n \leq 5$), the number density decreases rapidly with the cluster radius. As the cluster radius increases, the number density increases and reaches a maximum value at about $r = 2.6$nm. Beyond that, the number density decreases again with the cluster radius. This size distribution indicates that cluster coarsening takes place at this irradiation dose.

In Fig. 4, the precipitation kinetics are plotted for Cu clusters that contain more than 10 Cu atoms, which corresponds to a cluster radius of about 0.3 nm for a pure Cu cluster. This threshold value is chosen to be consistent with Ref. [18]. For the SANS experimental data shown in Fig. 4, the detection limit in terms of cluster radius is about 0.5 nm [9], which corresponds to about 45 Cu atoms in a pure Cu cluster. To determine how the choice of this threshold cluster size offsets the plots, Fig. 4 is replotted for Cu clusters containing more than 45 Cu atoms (or $r \geq 0.5$ nm), as shown in Fig. 7(a–b). Clearly the new threshold value only affects the plots in the nucleation and growth regime. In the coarsening regime, the plots are identical. This is because the majority of clusters have sizes greater than 0.5 nm during the coarsening stage, as can be seen in the cluster size distribution in Fig. 6. Therefore, using the same threshold value as in the SANS experiments (0.5 nm), the experimental validation of the precipitation kinetics is not affected.

So far all results presented here are based on the assumption that the Cu clusters contain 100% of Cu atoms. Previously, researchers have used SANS and APT techniques to discover that the Cu-rich precipitates (CRPs) in Fe are not pure Cu because they contain both Cu and Fe atoms and vacancies [9,10,34]. The concentration of Cu in the CRP determined in experiments may depend on many factors, including the artifact induced by ion trajectory aberrations in APT [34]. Morley et al. [34] removed the effects of trajectory aberration in their APT measurements and concluded that the Fe concentration in CRP is about 5–20%, which is lower than most reported values. Here an uncertainty analysis is conducted by assuming that the Cu concentration (f_{Cu}) in clusters is

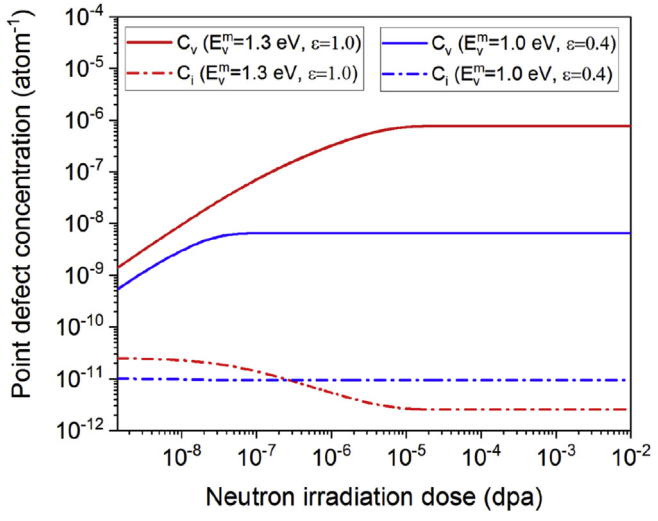

Fig. 5. Evolution of point defect concentration as a function of irradiation dose for two parameter sets. Same irradiation conditions and material properties are used for the two parameter sets: the dpa rate is 1.4×10^{-7} dpa/s, the dislocation density is 5×10^{13} m^{-2}, and the temperature is 300°C.

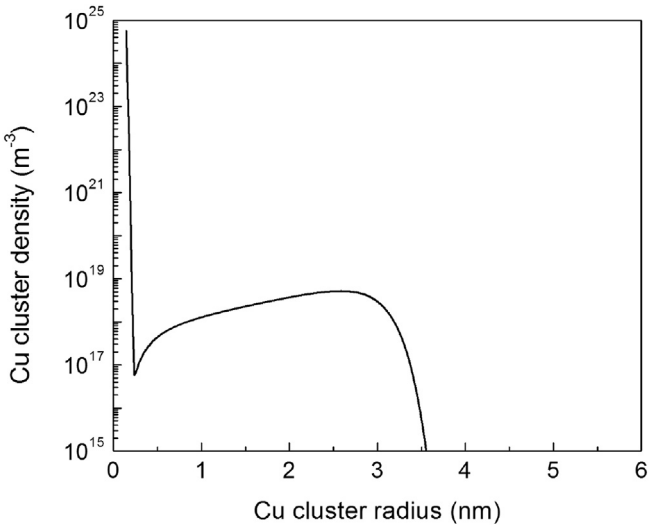

Fig. 6. Cu cluster size distribution at 0.14 dpa in a Fe-0.3 at.%Cu under neutron irradiation at 300°C.

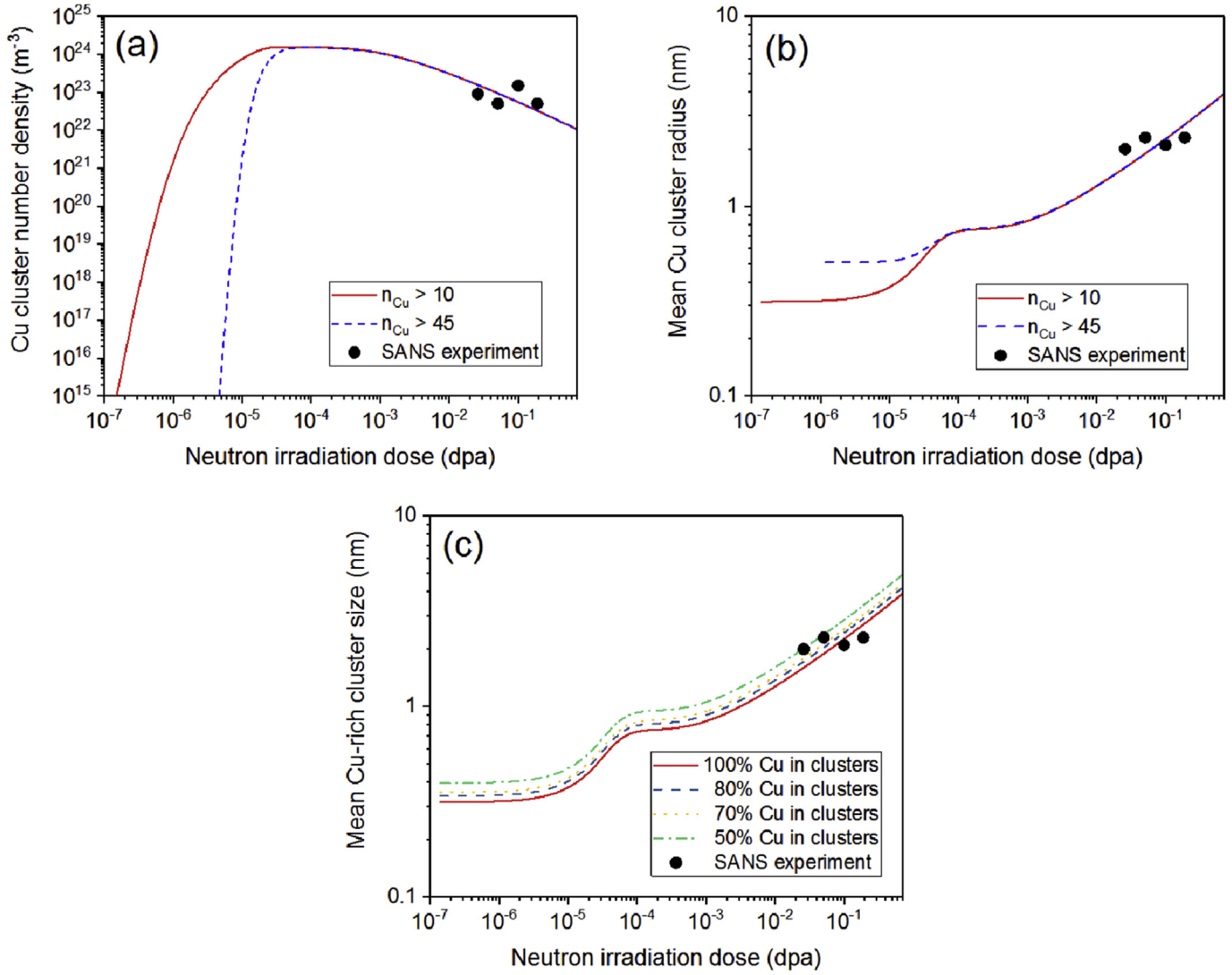

Fig. 7. Uncertainty analysis of the model for different experimental characterization criteria. (a–b) The precipitation kinetics plots using two threshold cluster sizes: $n_{Cu} = 10$ ($r = 0.3$ nm) and $n_{Cu} = 45$ ($r = 0.5$ nm). Here clusters are assumed to contain pure Cu atoms. (c) The evolution of Cu-rich precipitate (CRP) radius as a function of dose for different Cu concentration in CRP clusters.

50%, 70%, 80%, and 100%. Assuming an CRP contains n_{Cu} atoms, the total number of atoms and vacancies in the CRP is n_{Cu}/f_{Cu}. Since CRPs are coherent with the bcc Fe matrix, the atomic volume for both Cu and Fe atoms and vacancies in the CRP is V_{at}. Therefore, the radius of the CRP is

$$r_{CRP} = \left(\frac{3n_{Cu}V_{at}}{4\pi f_{Cu}}\right)^{1/3}. \quad (13)$$

The evolution of the CRP radius for different Cu concentration is shown in Fig. 7(c). When the Cu concentration in CRPs decreases, the CRP radius increases, but only slightly. Even if CRPs contain only 50% of Cu atoms, the CRP radius is still within the experimental data range. This is because r_{CRP} is proportional to $f_{Cu}^{-1/3}$ according to Eq. (13). Therefore, consideration of non-pure Cu clusters does not offset the evolution of Cu cluster radius significantly.

Another uncertainty is the definition of dpa in the neutron irradiation experiments. Unfortunately, no information is available about how the neutron irradiation doses were calculated in Refs. [2,9] where the SANS data are used for our validation. If the experimental dpa is defined based on the NRT model [35], the dose rate in experiments may be overestimated. For Fe, molecular dynamics simulations [36] showed that the dose rate is about 30% of the NRT rate [18]. If this is true, the curves shown in Fig. 4 would shift slightly to the left-hand side but still touch the experimental data points (not shown). The offsets correspond to a slightly overestimated coarsening kinetics and thus the model parameters should be adjusted slightly if the NRT dose rate is used.

4. Radiation hardening and embrittlement in Fe-0.3 at.%Cu

In Section 3, cluster dynamics predictions of the microstructural evolution during neutron irradiation in the Fe-0.3 at.%Cu alloy were shown. Predicted quantities of interest include the Cu cluster number density, mean cluster radius, and the cluster size distribution. In this section, such microstructural evolution information is connected to the change in mechanical properties such as yield strength. As mentioned earlier, Cu precipitates can become obstacles or pinning points for dislocation motion so that the yield strength of the alloy increases after the irradiation. This is the microscopic origin of radiation-induced precipitation hardening. To

make the connection between the precipitates and the hardening, dispersed barrier hardening models such as Orowan's model [37] are widely used. In the conventional Orowan's model, strengthening is achieved through the mechanism of dislocation bowing around spherical precipitates. The increase in the shear strength ($\Delta\tau_s$) is related to the number density (N) and diameter (d) of the precipitates:

$$\Delta\tau_s = \alpha\mu b(Nd)^{0.5} \tag{14}$$

where α is the obstacle or barrier strength with a value between 0 and 1; μ is the shear modulus of the matrix, for which a value of 82 GPa [21] is used for bcc Fe here; b is the Burgers vector of a dislocation, for which a value of $a_0\cdot\sqrt{3}/2$ is used for the a/2<111> dislocations. Many modifications have been proposed to add more physics to the original Orowan's model. For example, Kelly proposed a modified model [38] which considers (a) random distribution of particles in space, (b) finite size of particles, (c) more refined estimation of the dislocation line tension, and (d) the interaction between the two bow-out dislocations around the particle. Several other models were also derived from the original Orowan's model, such as Bacon-Kocks-Scattergood (BKS) model [39] and Friedel-Kroupa-Hirsch (FKH) model [40]. A systematic evaluation of these models is beyond the scope of this work so here only the Kelly's model is discussed. The Kelly's model has the form:

$$\Delta\tau_s = \alpha\frac{0.83\mu b}{\left[(Nd)^{-0.5} - d\right]}\cdot\frac{\ln(d/r_0)}{2\pi(1-\nu)^{0.5}}, \tag{15}$$

where α, μ, b, N, d have the same meanings as in Eq. (14); r_0 is the dislocation core radius; and ν is the Poisson's ratio. This model has been used by Hu et al. [21] for calculating the radiation hardening induced by dislocation loops and vacancy clusters. In this work this model is used for calculating the hardening induced by Cu clusters. The dislocation core radius is set to $r_0 = 3b$ (~0.75 nm) and Poisson's ratio is set to $\nu = 1/3$. Note in Eq. (15), the cluster diameter should be greater than r_0, $d > r_0$.

The obstacle strength α depends on the obstacle type, size, and possibly temperature [41,42]. Typically for the same type of precipitates at the same temperature, the smaller precipitates have less resistance to dislocation motion than larger precipitates [42]. To capture this size-dependent strengthening effect, the empirical equation proposed by Hu et al. [21] is used in this work,

$$\alpha = 1 - \exp\left[-\left(\frac{d}{d_{ref}}\right)^n\right], \tag{16}$$

where the reference cluster diameter $d_{ref} = 4$ nm and the exponent $n = 2$ are used here. The strength factor α changes from 0 to 1 as the precipitate diameter increases, as shown in Fig. 8.

The increase in shear strength is correlated to the increase in yield strength by a Taylor's factor M = 3.06 [13],

$$\Delta\sigma_y = M\Delta\tau_s. \tag{17}$$

Therefore, using Eqs. (15)–(17), the increase in the yield strength due to Cu precipitation can be calculated. Some input parameters for these equations are summarized in Table 3. The number density (N) and diameter (d) of the Cu precipitates can be obtained from cluster dynamics modeling as discussed in Section 3. Note that here N and d can be treated either for the total set of clusters or individual clusters. Therefore, two approaches are used to calculate the hardening in this work. In the first approach, the total number density of Cu clusters and the average cluster diameter, which are shown in Fig. 4 (note the radius in Fig. 4 should be converted to diameter), are used as N and d to calculate the effective hardening directly. In the second approach, the number density and diameter of each cluster size are used to calculate its individual hardening contribution ($\Delta\sigma_n$). The N and d of each cluster size can be obtained from the cluster size distribution (Fig. 6) at any given time. Once the individual hardening contribution from each cluster size is obtained, the overall hardening can be calculated based on a superposition law. The superposition law can be linear sum, square root of the quadratic sum, or a combination of them [43], although none of them has a clear physical basis. Consistent with Hu et al.'s work [21] for voids and dislocation loops, we also found that the linear sum superposition law overpredicts the strengthening behavior significantly. Therefore in this work the square root of the sum of the squares superposition law is used to predict the total hardening due to all clusters,

$$\Delta\sigma_y = \sqrt{\Delta\sigma_1^2 + \Delta\sigma_2^2 + \Delta\sigma_3^2 + \ldots}. \tag{18}$$

Using the two approaches, the evolution of radiation hardening as a function of the irradiation dose can be calculated, as shown in Fig. 9(a). It can be seen that the two approaches give very similar results, suggesting that Eq. (18) works very well in this work. In both approaches, the hardening increases with dose very rapidly at low doses and reaches a saturated value of about 230 MPa at the dose range that a RPV will typically receive during the 80-year service time (~0.2 dpa).

Lambrecht et al. [13] have measured the increase in the yield strength at different irradiation doses in a Fe-0.3at.%Cu alloy. However, the measured hardening includes the contribution from

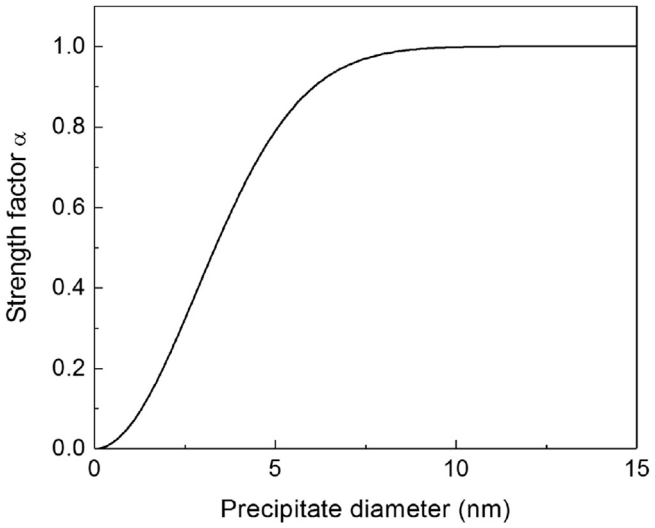

Fig. 8. The strength factor α as a function of Cu precipitate diameter.

Table 3
Input parameters for the modified Orowan's equation [Eqs. (15)–(17)].

Parameter	Value
μ, shear modulus	82 GPa
ν, Poisson's ratio	1/3
b, Burgers vector	$a_0\cdot\sqrt{3}/2$
r_0, dislocation core radius	3b
d_{ref}	4.0 nm
n	2.0
M, Taylor's factor	3.06

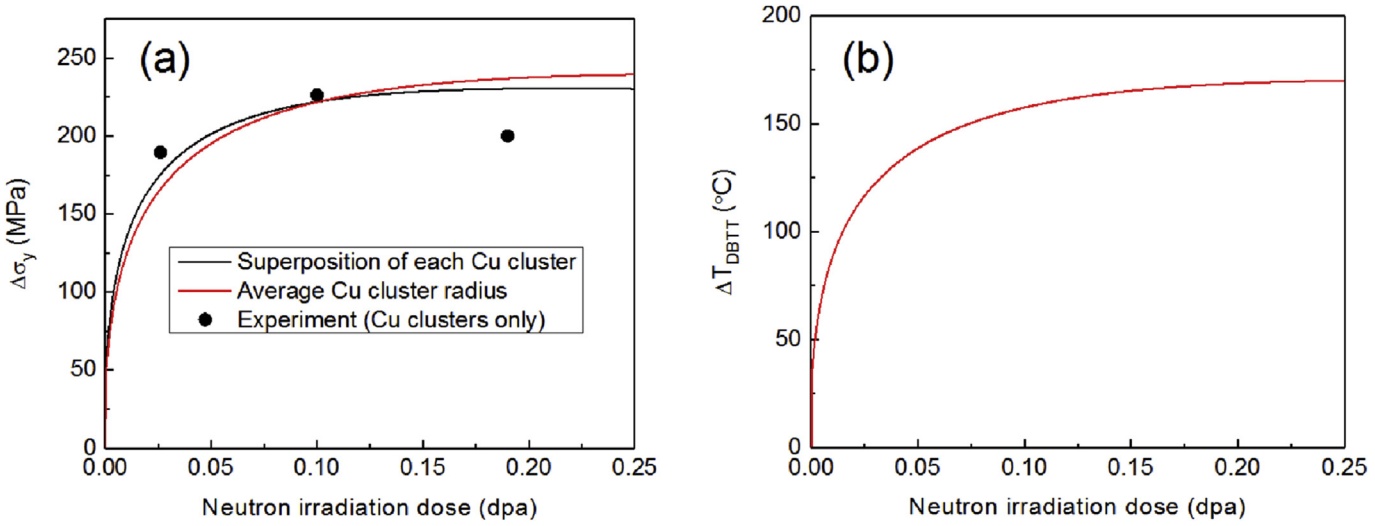

Fig. 9. Evolution of radiation hardening and embrittlement in a Fe-0.3at.%Cu alloy predicted by modeling. (a) Cu-cluster-induced hardening predicted by Kelly's model (lines), using the cluster dynamics simulation results as input for the model. The two approaches of calculating the hardening give similar results. Experimental results (filled circles) [13] are also shown for validation. (b) Predicted DBTT shift as a function of irradiation dose.

both Cu clusters and Fe matrix defect clusters because it is impossible to separate them in experiments. Therefore, for a fair comparison with our modeling work, which only considers the effect of Cu clusters, the contribution from matrix damage should be deducted. Here a reverse superposition law is applied to extract the net contribution from Cu clusters,

$$\Delta\sigma_{Cu} = \sqrt{\Delta\sigma_{Fe-Cu}^2 - \Delta\sigma_{Fe}^2}. \quad (19)$$

In Lambrecht et al.'s work [13], the hardening in a pure Fe was also reported at the same doses as in the Fe-Cu alloy. Here we assume that the matrix damage in the Fe-0.3at.%Cu alloy induces the same amount of hardening as in the pure Fe. Therefore the hardening solely due to the Cu cluster precipitation can be calculated using Eq. (19). The experimental data is shown as filled circles in Fig. 9(a). It can be seen that the modeling results agree well with the experimental results. Note that the above approach is a rough approximation because the Cu content in the alloy can cause the evolution of dislocation loops and vacancy clusters differently from that in pure Fe [2,12,44]. As a result, the hardening due to matrix damage in the FeCu alloy should be different from that in the pure Fe. Here a simple sensitivity analysis is conducted to evaluate how the uncertainty of $\Delta\sigma_{Fe}$ affects the result of $\Delta\sigma_{Cu}$. If the $\Delta\sigma_{Fe-Cu} = 250$ MPa for total hardening and $\Delta\sigma_{Fe} = 100$ MPa for Fe matrix hardening, $\Delta\sigma_{Cu} = 229$ MPa according to Eq. (19). If $\Delta\sigma_{Fe} = 120$ MPa, then $\Delta\sigma_{Cu} = 219$ MPa. If $\Delta\sigma_{Fe} = 80$ MPa, then $\Delta\sigma_{Cu} = 237$ MPa. In both cases, $\Delta\sigma_{Cu}$ varies about half the variation of $\Delta\sigma_{Fe}$ due to the square root of the quadratic sum nature of Eq. (19). Therefore, the above assumption is acceptable for the present study.

Based on the analysis of extensive experimental data, Eason et al. [4,8] found that the ductile-to-brittle transition temperature (DBTT) shift correlates strongly with the increase in yield strength. The relation between them can be approximated as a linear dependence by

$$\Delta T_{DBTT} = 0.71 \cdot \Delta\sigma_y, \quad (20)$$

where ΔT_{DBTT} is the change in the ductile-to-brittle transition temperature in degrees C. Based on the hardening evolution calculated from the first approach (i.e., using the total number density and average diameter of all clusters), the evolution of the DBTT shift can be predicted as a function of irradiation dose using Eq. (20), as shown in Fig. 9(b). The DBTT shift increases rapidly at low doses and saturates at about 170°C at high doses.

5. Conclusions and discussion

In this work, cluster dynamics modeling is used to model Cu cluster precipitation in a dilute Fe-0.3at.%Cu alloy under neutron irradiation at 300°C. The model is adapted from a previously proposed model [18] for Cu precipitation in a high-Cu alloy (Fe-1.34at.% Cu) under electron irradiation. We modified this model considering two effects: the in-cascade Frenkel pair recombination effect during neutron irradiation and solute trapping effect on vacancy diffusion. The later effect is found to play a major role in the coarsening kinetics. The results predicted by our modified model agree well with the precipitation kinetics measured by small angle neutron scattering experiments [2,9], for both the number density and mean radius of Cu clusters. The results also show that the homogenous precipitation mechanism can still be assumed for the Cu precipitation in the dilute Fe-0.3at.%Cu alloy. The characteristics of Cu precipitates (number density, radius, size distribution) predicted by the cluster dynamics modeling are used as input for a modified Orowan's hardening model to predict the evolution of precipitation hardening during neutron irradiation. The size-dependent obstacle strength is included in the hardening model. A superposition law of square root of the quadratic sum is used to account for the contribution from different sized clusters to the overall hardening. The predicted hardening agrees well with the experimental results of the same alloy under the same irradiation conditions in literature. Finally the shift in the ductile-to-brittle transition temperature is predicted as a function of irradiation dose. The results from this work may be used to understand the precipitation kinetics of Cu-rich clusters and the accompanying radiation hardening and embrittlement in realistic reactor vessel steels which contain dilute Cu. The model may also be adapted to study precipitation hardening in other alloys under irradiation or thermal aging conditions.

Our cluster dynamics model is adapted from a literature model that was used to study Cu precipitation in a high-Cu Fe based alloy of distinct materials properties and under different irradiation

conditions, as shown in Table 2. However, we showed that only two parameters need to be adjusted and both adjustments can be well justified. This success suggests that the model is relatively robust and it has the potential to predict the Cu precipitation kinetics for other Fe-Cu alloys of different composition and under different irradiation conditions. Despite this initial success, there are still many areas for further improvement of the model. In experiments, it has been found that the Cu precipitates are Cu-rich clusters [45]. However, in our modeling work the clusters are assumed to be pure Cu clusters. Although an uncertainty analysis is conducted to evaluate how non-pure Cu clusters offset the mean cluster radius (note the offset is small), the nucleation of the Cu-rich clusters is not explicitly modeled. The Cu clusters can transform to a 9R structure and the stable fcc structure as the cluster size increases [25–27]. Previous modeling work shows that the inclusion of such phase transformation mechanisms can improve the robustness of the precipitation model [25]. In this work such phase transformation mechanisms are not considered because the mean size of the Cu clusters is small in a dilute alloy. However, inclusion of the phase transformation may make the model to be applicable for a wide range of compositions. Previous kinetic Monte Carlo work [17] shows that small-size Cu clusters may be mobile. In this work, only Cu monomers are assumed to be diffusive so that the contribution of Cu cluster diffusion to the total Cu diffusivity is effectively included in the Cu monomer diffusion. However, explicit inclusion of Cu cluster diffusion [19] may improve the robustness of the model. In addition, in this work only homogenous Cu precipitation is considered. In reality heterogeneous precipitation of Cu at pre-existing dislocations and irradiation induced defect clusters may also take place, affecting precipitation kinetics [24]. In particular, the heterogeneous precipitation may be the dominant mechanism for Cu precipitation in Fe-based alloys containing less than 0.1 at.% Cu [24]. Such heterogeneous precipitation is thermodynamically preferred at various types of defects and has been demonstrated in an earlier work using Metropolis Monte Carlo [46]. This effect may be considered in the future by using cluster dynamics for solute precipitation.

The vacancy concentration under irradiation, which is directly used to calculate the radiation enhanced copper diffusivity, is obtained from a simple rate theory model. In this model, only defect production, defect recombination, and defect loss to dislocations are considered. The defect clustering effect is not considered. It has been shown that the inclusion of the defect clustering does not affect the late-stage coarsening kinetics, but it slows down the early-stage precipitation kinetics (i.e., nucleation and growth) [18]. Currently the experimental precipitation kinetics data are only available in the late-stage coarsening regime (Figs. 3 and 4). Therefore, experimental data on the early-stage precipitation kinetics can be very helpful for validating the cluster dynamics model. However, the time in this stage is short and reliable experimental data may not be obtained accurately. Alternatively, other modeling methods such as Kinetic Monte Carlo modeling may provide valuable information in this regime.

The radiation hardening due to Cu precipitates is predicted by a modified Orowan's hardening model. A size-dependent obstacle strengthening factor [Eq. (16)] is used to account for the different resistance to dislocation motion from various sized precipitates. The reference cluster diameter (d_{ref}) and the exponent (n) in this model are empirically chosen parameters. Molecular dynamics simulations may provide more science-based justification for choosing these parameters. The predicted hardening in this work only includes the contribution from Cu clusters. The matrix defect structures (dislocation loops, voids, etc.) and other types of precipitates (e.g., Mn-Ni-Si) are not included in the current model. To develop more predictive models for predicting the radiation hardening and embrittlement in realistic RPV steels, the contributions from these other types of clusters should also be included in the future.

Acknowledgements

This work is supported by the DOE Office of Nuclear Energy Light Water Reactor Sustainability (LWRS) Program. X.M.B. would like to thank the financial support from Battelle Energy Alliance (Idaho National Laboratory) to Virginia Tech through the Grizzly Project (Fund #418112) and the Faculty Joint Appointment Program (Fund #418132). The authors acknowledge the use of the computing facilities at the High Performance Computing at Idaho National Laboratory and the Advanced Research Computing at Virginia Tech. This manuscript has been co-authored by Battelle Energy Alliance, LLC under Contract No. DE-AC07-05ID14517 with the U.S. Department of Energy. The United States Government retains and the publisher, by accepting the article for publication, acknowledges that the United States Government retains a nonexclusive, paid-up, irrevocable, world-wide license to publish or reproduce the published form of this manuscript, or allow others to do so, for United States Government purposes.

References

[1] C. English, J. Hyde, 4.05-Radiation damage of reactor pressure vessel steels A2-konings, in: J.M. Rudy (Ed.), Comprehensive Nuclear Materials, Elsevier, Oxford, 2012, p. 151.
[2] E. Meslin, et al., Characterization of neutron-irradiated ferritic model alloys and a RPV steel from combined APT, SANS, TEM and PAS analyses, J. Nucl. Mater. 406 (2010) 73.
[3] K. Farrell, T.S. Byun, N. Hashimoto, Deformation mode maps for tensile deformation of neutron-irradiated structural alloys, J. Nucl. Mater. 335 (2004) 471.
[4] E.D. Eason, G.R. Odette, R.K. Nanstad, T. Yamamoto, A physically-based correlation of irradiation-induced transition temperature shifts for RPV steels, J. Nucl. Mater. 433 (2013) 240.
[5] G.R. Odette, G.E. Lucas, Recent progress in understanding reactor pressure vessel steel embrittlement, Radiat. Eff. Defects Solids 144 (1998) 189.
[6] G. Salje, M. Fellerkniepmeier, Diffusion and solubility of copper in iron, J. Appl. Phys. 48 (1977) 1833.
[7] P.B. Wells, et al., Evolution of manganese–nickel–silicon-dominated phases in highly irradiated reactor pressure vessel steels, Acta Mater. 80 (2014) 205.
[8] E.D. Eason, G.R. Odette, R.K. Nanstad, S. Yamamoto, A Physically Based Correlation of Irradiation-induced Transition Temperature Shifts for RPV Steels, Oak Ridge Report ORNL/TM-2006/530, 2007.
[9] F. Bergner, M. Lambrecht, A. Ulbricht, A. Almazouzi, Comparative small-angle neutron scattering study of neutron-irradiated Fe, Fe-based alloys and a pressure vessel steel, J. Nucl. Mater. 399 (2010) 129.
[10] E. Meslin, B. Radiguet, P. Pareige, A. Barbu, Kinetic of solute clustering in neutron irradiated ferritic model alloys and a French pressure vessel steel investigated by atom probe tomography, J. Nucl. Mater. 399 (2010) 137.
[11] M. Lambrecht, A. Almazouzi, Positron annihilation study of neutron irradiated model alloys and of a reactor pressure vessel steel, J. Nucl. Mater. 385 (2009) 334.
[12] M. Hernández-Mayoral, D. Gómez-Briceño, Transmission electron microscopy study on neutron irradiated pure iron and RPV model alloys, J. Nucl. Mater. 399 (2010) 146.
[13] M. Lambrecht, et al., On the correlation between irradiation-induced microstructural features and the hardening of reactor pressure vessel steels, J. Nucl. Mater. 406 (2010) 84.
[14] G.R. Odette, T. Yamamoto, D. Klingensmith, On the effect of dose rate on irradiation hardening of RPV steels, Philos. Mag. 85 (2005) 779.
[15] F. Soisson, et al., Atomistic Kinetic Monte Carlo studies of microchemical evolutions driven by diffusion processes under irradiation, J. Nucl. Mater. 406 (2010) 55.
[16] C.S. Becquart, B.D. Wirth, 1.14-Kinetic Monte Carlo simulations of irradiation effects, in: R.J.M. Konings (Ed.), Comprehensive Nuclear Materials, Elsevier, Oxford, 2012, p. 393.
[17] F. Soisson, C.C. Fu, Cu-precipitation kinetics in alpha-Fe from atomistic simulations: vacancy-trapping effects and Cu-cluster mobility, Phys. Rev. B 76 (2007) 214102.
[18] F. Christien, A. Barbu, Modelling of copper precipitation in iron during thermal aging and irradiation, J. Nucl. Mater. 324 (2004) 90.
[19] T. Jourdan, F. Soisson, E. Clouet, A. Barbu, Influence of cluster mobility on Cu precipitation in α-Fe: a cluster dynamics modeling, Acta Mater. 58 (2010) 3400.

[20] S.I. Golubov, A.V. Barashev, R.E. Stoller, Radiation damage theory, in: R.J.M. Konings (Ed.), Comprehensive Nuclear Materials, Elsevier, Oxford, 2012, p. 357.
[21] X. Hu, D. Xu, T.S. Byun, B.D. Wirth, Modeling of irradiation hardening of iron after low-dose and low-temperature neutron irradiation, Model. Simul. Mater. Sci. Eng. 22 (2014) 065002.
[22] R.E. Stoller, S.I. Golubov, C. Domain, C.S. Becquart, Mean field rate theory and object kinetic Monte Carlo: a comparison of kinetic models, J. Nucl. Mater. 382 (2008) 77.
[23] A. Hardouin Duparc, C. Moingeon, N. Smetniansky-de-Grande, A. Barbu, Microstructure modelling of ferritic alloys under high flux 1 MeV electron irradiations, J. Nucl. Mater. 302 (2002) 143.
[24] B. Radiguet, A. Barbu, P. Pareige, Understanding of copper precipitation under electron or ion irradiations in FeCu0.1 wt% ferritic alloy by combination of experiments and modelling, J. Nucl. Mater. 360 (2007) 104.
[25] G. Stechauner, E. Kozeschnik, Thermo-kinetic modeling of Cu precipitation in α-Fe, Acta Mater. 100 (2015) 135.
[26] P.J. Othen, M.L. Jenkins, G.D.W. Smith, W.J. Phythian, Transmission electron microscope investigations of the structure of copper precipitates in thermally-aged Fe—Cu and Fe—Cu—Ni, Philos. Mag. Lett. 64 (1991) 383.
[27] P.J. Othen, M.L. Jenkins, G.D.W. Smith, High-resolution electron microscopy studies of the structure of Cu precipitates in α-Fe, Philos. Mag. A 70 (1994) 1.
[28] M.H. Mathon, et al., Experimental study and modelling of copper precipitation under electron irradiation in dilute FeCu binary alloys, J. Nucl. Mater. 245 (1997) 224.
[29] L. Malerba, et al., Comparison of empirical interatomic potentials for iron applied to radiation damage studies, J. Nucl. Mater. 406 (2010) 19.
[30] https://computation.llnl.gov/projects/sundials.
[31] S.I. Golubov, A.M. Ovcharenko, A.V. Barashev, B.N. Singh, Grouping method for the approximate solution of a kinetic equation describing the evolution of point-defect clusters, Philos. Mag. A 81 (2001) 643.
[32] G.S. Was, T. Allen, Radiation-induced segregation in multicomponent alloys: effect of particle type, Mater. Charact. 32 (1994) 239.
[33] E. Meslin, et al., Cluster-dynamics modelling of defects in α-iron under cascade damage conditions, J. Nucl. Mater. 382 (2008) 190.
[34] A. Morley, et al., Determining the composition of small features in atom probe: bcc Cu-rich precipitates in an Fe-rich matrix, Ultramicroscopy 109 (2009) 535.
[35] M.J. Norgett, M.T. Robinson, I.M. Torrens, A proposed method of calculating displacement dose rates, Nucl. Eng. Des. 33 (1975) 50.
[36] D.J. Bacon, A.F. Calder, F. Gao, Defect production due to displacement cascades in metals as revealed by computer simulation, J. Nucl. Mater. 251 (1997) 1.
[37] E. Orowan, Symposium on Internal Stresses in Metals and Alloys (Institute of Metals, 1948).
[38] P.M. Kelly, Progress report on recent advances in physical metallurgy: (C) the quantitative relationship between microstructure and properties in two-phase alloys, Int. Metall. Rev. 18 (1973) 31.
[39] D.J. Bacon, U.F. Kocks, R.O. Scattergood, The effect of dislocation self-interaction on the orowan stress, Philos. Mag. 28 (1973) 1241.
[40] F. Kroupa, P.B. Hirsch, Elastic interaction between prismatic dislocation loops and straight dislocations, Discuss. Faraday Soc. 38 (1964) 49.
[41] P.M. Rice, S.J. Zinkle, Temperature dependence of the radiation damage microstructure in V–4Cr–4Ti neutron irradiated to low dose, J. Nucl. Mater. 258–263 (1998) 1414. Part 2.
[42] D.J. Bacon, Y.N. Osetsky, D. Rodney, Chapter 88 dislocation–obstacle interactions at the atomic level, in: J.P. Hirth, L. Kubin (Eds.), Dislocations in Solids, Elsevier, 2009, p. 1.
[43] G.R. Odette, G.E. Lucas, G. Tedeski, B.D. Wirth, Development of Superposition Rules for Hardening in Alloys Containing Multiple Defect Populations, Fusion Materials Semiannual Progress Report for Period Ending 25 (DOE/ER-0313/25) vol. 221, 1998.
[44] F. Bergner, A. Ulbricht, M. Hernandez-Mayoral, P.K. Pranzas, Small-angle neutron scattering study of neutron-irradiated iron and an iron–nickel alloy, J. Nucl. Mater. 374 (2008) 334.
[45] R. Prakash Kolli, D.N. Seidman, The temporal evolution of the decomposition of a concentrated multicomponent Fe–Cu-based steel, Acta Mater. 56 (2008) 2073.
[46] Y. Zhang, et al., Preferential Cu precipitation at extended defects in bcc Fe: an atomistic study, Comput. Mater. Sci. 101 (2015) 181.